Applied Energy Symposium 2021: Low carbon cities and urban energy systems
September 4-8, 2021, Matsue, Japan
Paper ID: 91

Performance enhancement of perovskite solar cell using Al-TiO_2 thin film as electron transporting buffer layer

D.I. Kim[1], J.W. Lee[1,2], R.H. Jeong[1,2], S. Park[1,2], K.-H. Hwang[1,2], S.-H. Nam[2] and Jin-Hyo Boo[1,2*]

[1]Department of Chemistry, Sungkyunkwan University, Suwon 440-746, South Korea
[2]Institue of Basic Science, Sungkyunkwan University, Suwon 440-746, South Korea

ABSTRACT

It is important to prevent the decomposition of perovskite by UV-radiation in air environment for commercialization. The structure of a mesoscopic perovskite solar cell has great potential for the solar cell industry. It is vulnerable to UV-radiation due to reversible performance deterioration that has been observed in this structure. In this study, perovskite solar cells (PSCs) were prepared using an Al-doped TiO_2 buffer layer as electron transport layer combined with a mesoporous-TiO_2 layer in order to prevent this problem. The Al concentration of 7 mol% in Al-TiOx buffer layer was shown to enhance the performance of the perovskite solar cell, as these solar cells exhibited a power conversion efficiency of up to 11.87%.

Keywords: Perovskite solar cell, Photovoltaics, Buffer layer, Electron transport layer

1. INTRODUCTION

Separated charges each have different electrode arrival carrier mobility owing to some electron transferred from perovskite to MP-TiO_2 which uses less than 50 nm pore size, being trapped and detrapped in the Mesoscopic structure. The above-mentioned phenomenon leads to I-V hysteresis. In order to overcome this problem, efforts have been made to achieve high performance and stability for the scan direction and speed to reduce the hysteresis of the I-V curve. Therefore, there is a demand for low trap density, high conductivity and mobility by changing the surface morphology of the ETL. Related studies, such as those examing nanorods [1], dendritic structure [2], nanowire structure [3], nano tube [4], floral patterns [5], and inverse opal [6] were conducted it attempts to solve these problems. Another alternative idea, involved changing the property of ETL by replacing other metal ions such as ZnO [7], Zn_2SnO_4 [8], NiO [9], CuO [10], and SnO [11]. Some metal oxides doped with hetero metal ions include Li-doped TiO_2 [12], Zn-doped TiO_2 [13], Nb-doped TiO_2 [14], Alkali-doped TiO_2 [15], and Sn-doped TiO_2 [16]. The doping method of metal oxide has been approached in various ways in the past. These metal ions are an especially promising material, due to their large band gap, high conductivity and reduced sensitivity to ultraviolet light. This effort has reduced the hysteresis of the I-V response and has obtained high PCE. The effects of aluminum doping TiO_2 have already been reported in various fields. Al^{3+} ion penetrates into TiO_2 in the aluminum doping process through substitution, resulting in the appearance of new energy levels that can affect the charge transport property in semiconductors [17]. According to the density functional theory calculations, it was reported that the holes are strongly localized in the O 2p nonbonding orbital of a three-coordinated O ion. Dopants reduce carrier mobility due to photogenerated carriers being trapped by extrinsic defects [18]. However, replacing the MP-TiO_2 with an insulating material such as Al_2O_3 increases the open-circuit voltage. Non-stoichiometric TiO_2 existence has deep electron trap sites, thus reducing the splitting of the quasi Fermi-energy level.

Solar cells work based on the photoelectric effect. When solar light enters the solar cell, the carriers in the valence band absorb photon energy greater than the energy band gap of material, and the electrons and the

Selection and peer-review under responsibility of the scientific committee of CUE2021

holes are separated, and the electrons are excited to the conduction band. If photon energy absorption occurs in the spatial region of the p-n junction, electrons move to p-type region and holes move to n-type region through depletion region by drift due to the electric field formed inside. This phenomenon causes current and voltage to be generated from the separation of at quasi Fermi-energy level formed by p-type and n-type semiconductor junction.

When light reaches the perovskite material, electron-hole pairs are created in the material and inject carriers into the charge transport layer **(figure 1)**. Charge separation and injection can occur in the perovskite through two pathways: electrons are injected into electron transport layer (ETL) (Equation-1a) and holes are injected into the hole transport layer (HTL) (Equation-2a). The carrier injected into the charge transport layer lead to exciton annihilation by photoluminescence (PL) (Equation-3) or non-radiative recombination (Equation-4). Back charge transfer occurs at ETL/perovskite layer interface (Equation-5) and perovskite layer/HTL interface (Equation-6). Charge recombination occurs by recombination of electrons in the ETL and holes in the HTL (Equation-7). Due to equations 3, 4, 5, 6, and 7 degrade the efficiency of PSCs, the carrier lifetime of perovskite should be long.

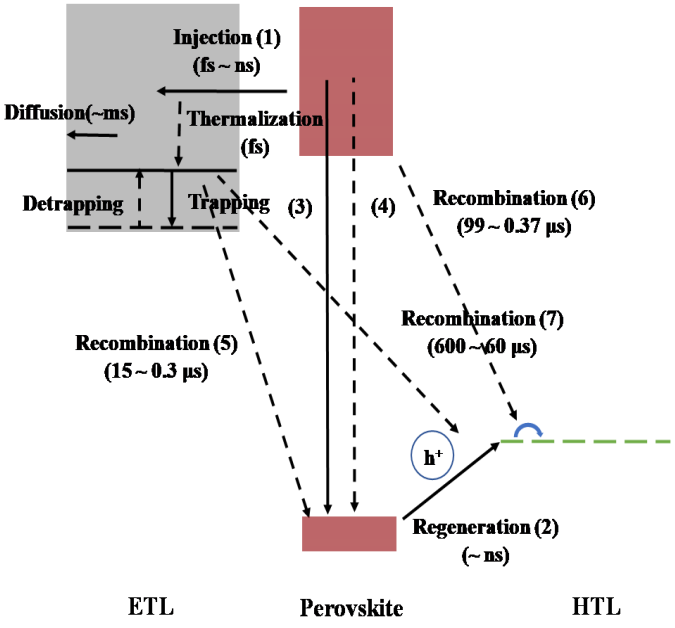

Figure 1. Schematic diagram of carrier transfer processes in perovskite solar cells (PSCs).

Electrons are injected into ETL

$(e^- \text{ --- } h^+)$perovskite → e_{cb}^- (ETL) + h^+ (perovskite)

(Equation-1a)

h^+ (perovskite) → h^+ (HTL) **(Equation-1b)**

Holes are injected into the HTL

$(e^- \text{ --- } h^+)$perovskite → h^+ (HTL) + e^-(perovskite)

(Equation-2a)

e^-(perovskite) → e_{cb}^- (ETL) **(Equation-2b)**

Exciton annihilation

$(e^- \text{ --- } h^+)$perovskite → photoluminescence

(Equation-3)

$(e^- \text{ --- } h^+)$perovskite → non-radiative recombination

(Equation-4)

Back charge transfer

e_{cb}^- (ETL) + h^+ (perovskite) → recombination

(Equation-5)

h^+ (HTL) + e^-(perovskite) → recombination

(Equation-6)

Charge recombination occurs

e_{cb}^- (ETL) + h^+ (HTL) → recombination **(Equation-7)**

As the recombination rate of charge decreases, the efficiency of the PSCs increases. The passivation effect is used to reduce charge recombination of $MAPbI_3$ extracted charges **(figure 2)**. $MAPbI_3$ has two interfaces. One is the interface between the ETL and the $MAPbI_3$ layer. The other is the interface between the $MAPbI_3$ layer and the HTL. It is important to reduce the recombination rate of electrons and holes at each interface. It is necessary to adjust the energy level of the conduction band and the valence band using self-passivation, doping process, and interlayer passivation.

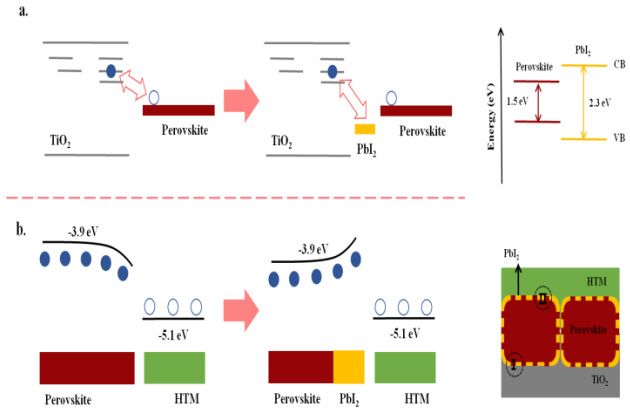

Figure 2. Passivation effect of perovskite solar cells (PSCs).

Here, we prepared PSCs with Al-TiO_2 as buffer layer in mesoscopic structure lead to passivation effect. Carrier recombination of buffer layer was reduced at buffer layer/$MAPbI_3$ interafec due to HOMO-enegy level

of ETL is increased. Buffer layer greatly also reduced interfacial resistance. V_{oc} was improved due to the band gap of Al-TiO_2 was wider and energy level of conduction band was enhanced. In particular, it showed the optimal conditions at 7 mol% Al-TiO_2 buffer layer. $MAPbI_3$ layer was deposited on the MP-TiO_2 combined with Al-buffer layer and cell performance was achieved 11.87%.

2. EXPERIMENTAL DETAILS

2.1 Synthesis of Al-doped TiO_2

Titanium precursor sol was prepared by adding 1.54 mL titanium (IV) isopropoxide (Sigma Aldrich, 99.999%) to 0.49 mL hydrochloric acid (35.0~37.0%) under vigorous stirring for 30 min. 16 mL of 2-propanol (IPA) add to Titanium precursor sol. After stirring, 0, 3, 5, 7 and 10 mol% aluminum isopropoxide (Sigma Aldrich, 98.00%) pre-cursor was added to previous solution for 3 h.

2.2 Fabrication of PSC

The FTO substrate was etched using ZnO powder and 2 M hydrochloric acid aqueous solution and cleaned with acetone and IPA for 10 min respectively. The substrate was dried with nitrogen and subjected to OPT. To prepare CP-TiO_2 on FTO substrate, 0.15 M titanium diisopropoxidebis (acetylacetonate) (Sigma-Aldrich, 75 wt%, in IPA) solution was coated by spin coating method, which was dried at 155 ℃. The MP-TiO_2 layer was deposited on CP-TiO_2/FTO using TiO_2 paste (Dyesol, DSL 18NR-tTiO_2). In order to make a buffer layer, Al-doped TiO_2 solution was coated by spin coating method, which was dried at 125 ℃ and then annealed at 500 ℃ for 1 h. To obtain the $MAPbI_3$ film, 1 M PbI_2 (467 mg / mL, in DMF) and CH_3NH_3I (7 mg / mL, in IPA) were deposited on the mp-TiO_2 layer sequentially, which was dried at 100 ℃. The HTL was [contained 28.8 µL of Spiro-MeOTAD (Lumtec) (72.3 mg / mL in chlorobenzene), 4-tert-butylpyridine (Sigma-Aldrich, 96% The TSFI stock solution (Sigma-Aldrich, 99.8%) was stirred for 24 h deposited on the $MAPbI_3$ layer. A gold electrode was thermally evaporated on the HTL.

2.3 Characterization

Film XRD (Bruker D8 Advance system) measurement was performed using Cu Kα radiation (λ=1.5416 Å) with a 40 kV beam voltage and a 30 mA beam current. SEM was performed using a JEOL, JSM-7100F under 15 keV at 7.12×10^{-7} Torr. The optical absorbance characteristic was recorded using a UV-vis-NIR spectrometer (Shimadzu, UV-3600) in the wavelength range of 300-900 nm. The PL was measured by utilizing Fluorescence Spectrometer FluroMate (FS-2) under an excitation laser with a wavelength of 570 nm. J-V curves (SUN 2000) were measured using a xenon lamp under AM 1.5 filter at 100 mW/cm^2 illuminations in open circuit conditions. Electrochemical impedance spectroscopy (EIS) was performed in a frequency range from 1 MHz to 100 mHz using an SUN 2000 Instruments under AC voltage with a perturbation amplitude of 10 mV was applied in the EIS measurement.

3. RESULTS AND DISCUSSION

Figure 3 illustrates each device structure used in this study, where non-porous TiO_2, MP-TiO_2 and buffer layer are combined with electron acceptor between active layer and ETL. We prepared with mesoscopic PSC structure with the various selective contacts. All architectures will show the collect of different electrons. Generated electron has different mobility while passing the ETL due to trap sites of electron are different because of nonporous-TiO_2, MP-TiO_2 and buffer layer. We have studied the 4 type structures shown in **figure 3**, which was find out which structure is best.

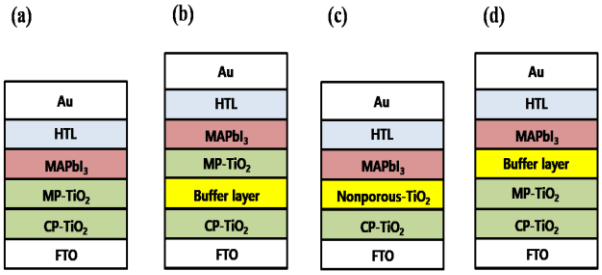

Figure 3. Device architectures with different buffer layer or non-porous TiO_2 layer in mesoscopic structure. (a)FTO/CP-TiO_2/MP-TiO_2/ $MAPbI_3$/HTL/Au (b)FTO/CP-TiO_2/Buffer layer/MP-TiO_2/$MAPbI_3$/HTL/Au (c)FTO/CP-TiO_2/non-porous TiO_2/$MAPbI_3$/HTL/Au (d)FTO/CP-TiO_2/MP-TiO_2/ Buffer layer/$MAPBI_3$/HTL/Au

J–V curves of the all structures **(see figure 3)** were shown in **figure 4(a)** and summarized **in Table 1**. The structure (b) shows the best efficiency compared to other structures. It was confirmed that the J_{sc}, V_{oc}, and FF were improved compared with the other samples, and the cell efficiency was also improved. However, cell performance was dropped in the types (c) and (d). In

particular, it has been found that the FF of type (c) is reduced by about 20% compared with the other FF of devices, which is considered to be less stable.

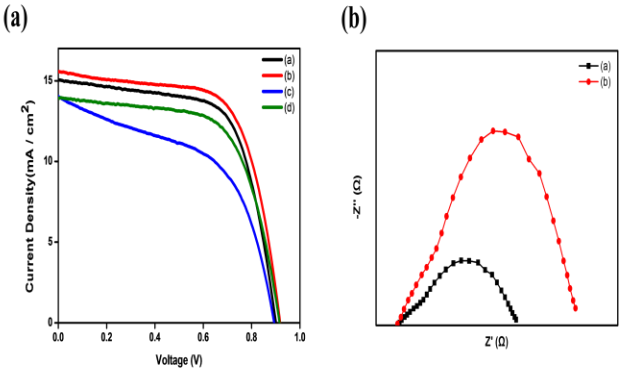

Figure 4. (a) J-V curves of mesoscopic PSCs with different type (b) Nyquist plots of mesoscopic PSCs with type FTO/CP-TiO_2/MP-TiO_2/ $MAPbI_3$/HTL/Au and FTO/CP-TiO_2/Buffer layer/MP-TiO_2/$MAPbI_3$/HTL/Au.

Table 1. PV performance parameters summarized J–V measurements with different architectures.

Sample no.	Jsc (mA/cm^2)	V_{oc} (V)	FF (%)	PCE (%)
(a)	14.66	0.8980	65.65	8.640
(b)	**15.12**	**0.9163**	**66.65**	**9.234**
(c)	12.84	0.9076	54.62	6.366
(d)	13.64	0.9126	64.72	8.055

In order to analyze the reasons for the enhanced efficiency and to understand the charge transfer behavior of the solar cells, EIS was measured. **Figure 4(b)** shows the Nyquist plots of Mesoscopic PSCs with (a) and (b) of low impedance frequency region. The EIS contains two RC arcs. One is related to the contact resistance of the interfaces at high frequency and the other is attributed to recombination resistance and chemical capacitance of the device at low frequency [19]. Thus, EIS results can supply the informations such as charge transfer resistance and recombination at the ETL/$MAPbI_3$ interfaces and $MAPbI_3$/counter electrode in the field of PSC. The structure (b) of PSC presents smaller series resistance and larger recombination resistance than base sample (a). This proves that the carrier transport ability was improved and the recombination rate of carrier was reduced for the device (b) due to buffer layer. This result corresponds to the V_{oc} difference in T**able 1**. It was guess that when TiO_2-buffer layer was combined with the MP-TiO_2, the trap site in the ETL was reduced thus leading to less recombination. On the other hand, the Fermi-energy level of ETL was increased due to a higher conduction band energy level compared with MP-TiO_2, which lead to a reduced recombination rate and an increased V_{oc}. Therefore, we conducted an XRD analysis and SEM analysis in order to know why the cell efficiency was decreased in the case of structures (c) and (d).

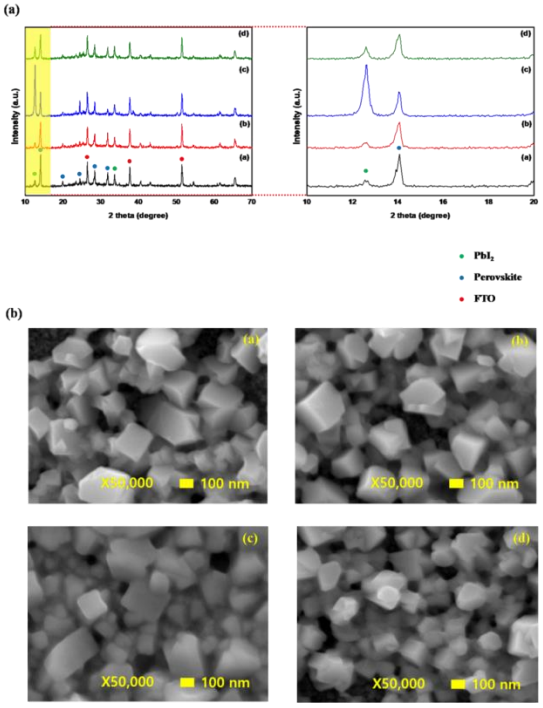

Figure 5. (a) XRD patterns and (b) SEM images of the $MAPbI_3$ layer with different type.

We made all structure of perovskite PSCs without HTL to confirme the XRD and SEM as shown in **figure 5**. **Figure 5(a)** show the XRD pattern of $MAPbI_3$ that revealed the intensity of PbI_2 at about 12° and the intensity of $MAPbI_3$ at about 14°, respectively. When the $MAPbI_3$ layer was fabricated on the ETL based types (a) and (b), no change was observed in the XRD results. However, the intensity of the $MAPbI_3$ peak was reduced and the intensity of PbI_2 peak was increased at samples (c) and (d). In particular, the peak intensity of PbI_2 was greatly increased in sample (c). Then, we confirmed that $MAPbI_3$ did not grow properly at structures (c) and (d), so that the PbI_2 and $MAPbI_3$ coexist in the active layer and the cell performance was deteriorated. The growth of $MAPbI_3$ crystal heavily depends on the thickness of non-porous TiO_2, which can be disturb by cause a defect of the $MAPbI_3$, which makes it less efficient than other type devices. These defects induce disability of carrier transfer ability and carrier recombination rate at the ETL/$MAPbI_3$ interfaces. **Figure 5(b)** showed SEM images

of $MAPbI_3$ film. Compared to the XRD results, morphology images of types (a) and (b) show the well growth of $MAPbI_3$ crystals. However, non-growing PbI_2 is bound between the crystal and the crystal in sample (c), and SEM image of sample (d) shows the intermediate state between samples (a) and (c).

We confirmed the change of the electron transper ability of carriers separated from the active layer through PL analysis in **figure 6**. The rate of carrier recombination is influenced by substance, structure and property of ETL. The area of the PL spectrum means the carrier recombination rate or carrier mobility. The results of PL are affected by both amount of exciton generation and mobility of carrier. The results showed that the area of the PL decreased in sample (b) compare to the other samples. This indicates that generated electrons can move smoothly to electrode through the $MAPbI_3$/ETL interface due to buffer layer. That is, the carrier lifetime was increased as recombination resistance was also increased. As a result, it can be seen that when the PSC was made using buffer layer, the ability of electron acceptor was enhanced, as comfirmed by the PL and EIS analysis. On the other hand, crystals do not grow properly because of this electrons can not be generated properly in the (c) and (d) structures. In a crystal that has not grown properly, electron and hole separation does not occur properly, so charge injection (Equation-1 and -2), bach charge transper (Equation-5 and -6) and charge recombnation (Equation-7) is not possible, and exciton annihilation (Equation-3 and -4) will happen at a very high speed. These results adversely affect the recombination rate, ETL and cell performance.

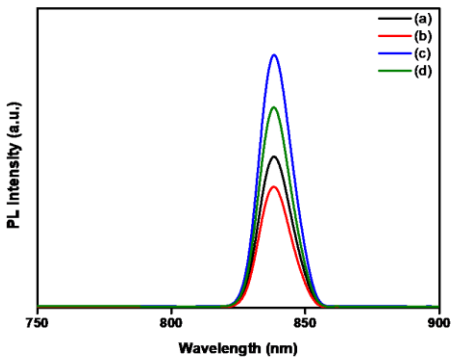

Figure 6. PL of $MAPbI_3$ films with different type.

When oxygen vacancies or Ti interstitials occur in the TiO_2 lattice, Ti ions are substituted for Al ions. Ti(IV) transforms to both Ti(III) and $Ti(IV)^+ + e^-$ forms due to defect site. Ti (III) is replaced by Al(III) which is relatively more stable. As mentioned above, the Al-doped TiO_2 buffer layer is beneficial to the enhancement of recombination resistance. We measured the photovoltaic performance of PSCs. The parameters of PV performance are summarized in T**able 4-2**. As shown in **figure 7(a)**, J_{sc}, V_{oc}, and FF was increased gradually until Al 7 mol% doping concentration, which contribute to improved cell performance from 9.234% to 11.87%. As the concentration of Al doping increases, the electrons transfer well from the $MAPbI_3$ layer to electrode through the ETL. The ability of electron acceptor was enhanced by doping process. As a result, V_{oc} was increased due to the Fermi-energy level was also increased and rate of recombination was reduced. When comparing the J-V results with the electrochemical impedance spectroscopy in **figure 7(b)**, 10 mol% Al doing sample of PSC increased series resistance and reduced recombination resistance than 7 mol% Al doping sample. It means that the carrier transport ability was decreased due to the Fermi-energy level of ETL was high that the electrons cannot go over energy barrier. Exciton annihilation (Equation-3 and -4) and back charge transper (Equation-6) rather than injection of electrons will absolutely occur. As a result, the electrons recombine with the hole. As the amount of Al doping increases, the HOMO-energy level of ETL will gradually increase, which will infer from the ABS results. The Al 7 mol% doping sample shows the most efficient charge injection (Equation-1) and low back charge transper (Equation-5) due to passivation effect. Therefore, we confirmed that the cell parameters of Al 7 mol% doping sample were improved and the best cell performance was obtained 11.87% compared to the non-doping sample. However, the cell performance was dropped at the doping concentration of 10 mol%. This is attributed that an energy level of conduction band seems to be too high to make the electrons harder to move through the ETL, resulting in an increase the recombination rate.

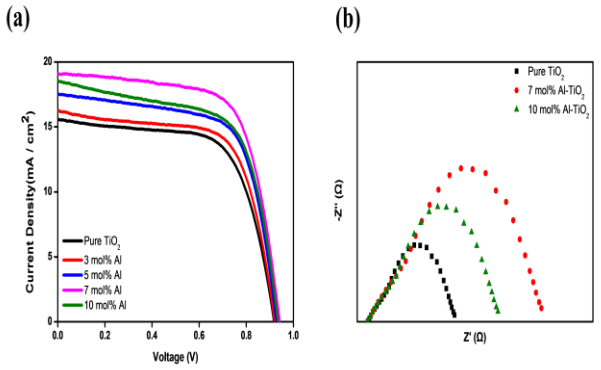

Figure 7. (a) J-V curves of Mesoscopic PSCs with different Al-doped TiO_2 buffer layer (0, 3, 5, 7, and 10 mol%). and (b) Nyquist plots of Mesoscopic PSCs with 0,7, and 10 mol% Al-doped TiO_2 buffer layer.

Table 2. Photovoltaic performance parameters summarized J–V measurements with different Al-doped TiO_2 buffer layer (0, 3, 5, 7, and 10 mol%).

Sample no.	Jsc (mA/cm^2)	Voc (V)	FF (%)	PCE (%)
Pure TiO_2	15.12	0.9163	66.65	9.234
3 mol% Al	15.63	0.9193	67.68	9.722
5 mol% Al	16.93	0.9274	67.84	10.66
7 mol% Al	**18.79**	**0.9405**	**67.14**	**11.87**
10 mol% Al	17.50	0.9343	67.30	11.00

4. CONCLUSION

The TiO_2 buffer layer for the fabrication of mesoscopic PSCs introduced provides a means to enhance excellent PV performance. Our studies approach to the reduce the interfacial resistance and increase the recombination resistance. The energy level of conduction band was increased by Al-doping TiO_2 to induce electrons to reach the electrode well. We obtained the efficiency of 11.87% with the PSC using a Al 7 mol% doping TiO_2 buffer layer to controlled the interfacial resistance and it influence cell parameter for good.

ACKNOWLEDGEMENT

This work was supported by the National Research Foundation of Korea (NRF) grant funded by the Korea government(MSIT). (2020R1A2C1011764)

REFERENCE

[1] H. S. Kim, J. W. Lee, N.Yantara, P. P. Boix, S. A. Kulkarni, S. Mhaisalkar, M.Gratzel, N. G. Park, High Efficiency Solid-State Sensitized Solar Cell-Based on Submicrometer Rutile TiO_2 Nanorod and $CH_3NH_3PbI_3$ Perovskite Sensitizer, *Nano Lett.* 13 (2013) 2412-2417.

[2] W. Q. Wu, F. Huang, D. Chen, Y. B. Cheng, R. A. Caruso, Thin Films of Dendritic Anatase Titania Nanowires Enable Effective Hole-Blocking and Efficient Light-Harvesting for High-Performance Mesoscopic Perovskite Solar Cells, *Adv. Funct. Mater.* 25 (2015) 3264-3272.

[3] J. H. Im, J. Luo, M. Franckevicius, N. Pellet, P. Gao, T. Moehl, S. M. Zakeeruddin, M. K. Nazeeruddin, M. Gratzel, N. G. Park, Nanowire Perovskite Solar Cell, *Nano Lett.* 15 (2015) 2120-2126.

[4] Xiaoyan Wanga, Zhen Lia, Wenjing Xuc, Sneha A. Kulkarnia, Sudip K. Batabyala, Sam Zhangd, Anyuan Caoc, Lydia Helena Wong, TiO_2 nanotube arrays based flexible perovskite solar cells with transparent carbon nanotube electrode, *Nano Energy* 11 (2015) 728-735.

[5] K. Girija, S. Thirumalairajan, A. K. Patra, D. Mangalaraj, Ponpandian, Viswanathan, Enhanced photocatalytic performance of novel self-assembled floral b-Ga_2O_3 nanorods, *Curr. Appl. Phys.* 13 (2016) 652-658.

[6] J. S. King, E. Graugnard, C. J. Summers, TiO_2 Inverse Opals Fabricated Using Low-Temperature Atomic Layer Deposition, *Adv. Mater.* 7 (2005) 1010-1013.

[7] Dae-Yong Son, Jeong-Hyeok Im, Hui-Seon Kim, Nam-Gyu Park, 11% Efficient Perovskite Solar Cell Based on ZnO Nanorods: An Effective Charge Collection System, *J. Phys. Chem. C* 118 (2014) 16567-16573.

[8] Lee Seul Oh, Dong Hoe Kim, Jin Ah Lee, Seong Sik Shin, Jin-Wook Lee, Ik Jae Park, Min Jae Ko, Nam-Gyu Park, Sung Gyu Pyo, Kug Sun Hong, Jin Young Kim, Zn_2SnO_4-Based Photoelectrodes for Organolead Halide Perovskite Solar Cells, *J. Phys. Chem. C* 118 (2014) 22991-22994.

[9] Long Hu, Jun Peng, Weiwei Wang, Zhe Xia, Jianyu Yuan, Jialing Lu, Xiaodong Huang, Wanli Ma, Huaibing Song, Wei Chen, Yi-Bing Cheng, Jiang Tang, Sequential Deposition of $CH_3NH_3PbI_3$ on Planar NiO Film for Efficient Planar Perovskite Solar Cells, *ACS Photonics* 7 (2014) 547-553.

[10] Chuantian Zuo, Liming Ding, Solution-Processed Cu_2O and CuO as Hole Transport Materials for Efficient Perovskite Solar Cells, *small* 11(2015) 5528-5532.

[11] Qi Jiang, Liuqi Zhang, Haolin Wang, Xiaolei Yang, Junhua Meng, Heng Liu, Zhigang Yin, Jinliang Wu, Xingwang Zhang, Jingbi You, Enhanced electron extraction using SnO_2 for high-efficiency planar-

structure $HC(NH_2)_2PbI_3$-based perovskite solar cells, *Nat. Energy* 2 (2016) 1-7.
[12] Fabrizio Giordano, Antonio Abate, Juan Pablo Correa Baena, Michael Saliba, Taisuke Matsui, Sang Hyuk Im, Shaik M. Zakeeruddin, Mohammad Khaja Nazeeruddin, Anders Hagfeldt, Michael Graetzel, Enhanced electronic properties in mesoporous TiO_2 via lithium doping for high-efficiency perovskite solar cells, Nat. Commun. 7 (2016) 1-6.
[13] Ming-Chung Wu, Shun-Hsiang Chan, Meng-Huan Jao, Wei-Fang Su, Enhanced short-circuit current density of perovskite solar cells using Zn-doped TiO_2 as electron transport layer, *Sol. Energy Mater. Sol. Cells* 157 (2016) 447-453.
[14] Youhei Numata, Ryo Ishikawa, Yoshitaka Sanehira, Atsushi Kogo, Hajime Shirai, Tsutomu Miyasaka, Nb-doped amorphous titanium oxide compact layer for formamidinium-based high efficiency perovskite solar cells by low-temperature fabrication, *J. Mater. Chem. A* 6 (2018) 9583-9591.
[15] Trilok Singh, Senol Öz, Alexander Sasinska, Robert Frohnhoven, Sanjay Mathur, Tsutomu Miyasaka, Sulfate-Assisted Interfacial Engineering for High Yield and Efficiency of Triple Cation Perovskite Solar Cells with Alkali-Doped TiO_2 Electron-Transporting Layers, *Adv. Funct. Mater.* 28 (2018) 1-10.
[16] Yan Xiang, Zhu Ma, Jia Zhuang, Honglin Lu, Chunyang Jia, Junsheng Luo, Haimin Li, Xiaowei Cheng, Enhanced Performance for Planar Perovskite Solar Cells with Samarium-Doped TiO_2 Compact Electron Transport Layers, *J. Phys. Chem. C* 121 (2017) 20150-20157.
[17] Heli Wang, Jianjun He, Gerrit Boschloo, Henrik Lindstro1m, Anders Hagfeldt, Sten-Eric Lindquist, Electrochemical Investigation of Traps in a Nanostructured TiO_2 Film, *J. Phys. Chem. B* 105 (2001) 2529-2533.
[18] Anna A. Murashkina, Aida V. Rudakova, Vladimir K. Ryabchuk, Konstantin V. Nikitin, Ruslan V. Mikhailov, Alexei V. Emeline, Detlef W. Bahnemann, Influence of the Dopant Concentration on the Photoelectrochemical Behavior of Al-Doped TiO_2, *J. Phys. Chem. C* 122 (2018) 7975−7981.
[19] Amalie Dualeh, Thomas Moehl, Nicolas Te´ treault, Joe¨ l Teuscher, Peng Gao, MohammadKhaja Nazeeruddin, Michael Gratzel, Impedance Spectroscopic Analysis of Lead Iodide Perovskite-Sensitized Solid-State Solar Cells, *ACS Nano* 8 (2014) 362-373.